Synthesis of beta alumina films using the process of chemical vapor deposition under lithium-rich atmosphere

Chen Chi[1,a,*]

[1]School of Chemical Engineering and Pharmacy, Wuhan Institute of Technology, Wuhan, China
[a]15327326216@163.com
*Corresponding author: Chen Chi

Abstract: This study demonstrates the growth of Li-β-alumina films by laser chemical vapor deposition and investigates the effects of deposition temperature (T_{dep}), molar ratio of Li/Al ($R_{Li/Al}$) and total pressure (P_{tot}) on the phase formation, microstructure, orientations and deposition rate (R_{dep}) of the film. Single-phase Li-β-alumina films were deposited at T_{dep} = 1100 K–1300 K, $R_{Li/Al}$ = 20–50 and P_{tot} = 600–1000 Pa. Li-β-alumina films with the hexagonally faceted platelet morphology (flake-like) were deposited at P_{tot} = 1000 Pa, whereas bulky grains were formed at P_{tot}=600 Pa. The maximum R_{dep} of Li-β-alumina films was 30 μm h^{-1} at T_{dep}=1225 K, $R_{Li/Al}$=30 and P_{tot}=600 Pa. At room temperature the ionic conductivity of Li-β-alumina film prepared by laser CVD reached 2×10^{-4} S/cm, demonstrating superior performance and significant potential in lithium battery.

Keywords: beta alumina; CVD; film; ionic conductivity; electrolyte

1. Introduction

Beta alumina was first reported by Rankin and Merwin in 1916 [1, 2]. However, at the beginning it was not realized that lithium or sodium is an essential constituent of this material. The beta alumina is actually a sodium aluminate and its crystal structure was first established by Bragg [3] in 1931 when beta alumina was assigned the formula $(Li/Na)_2O \cdot 11Al_2O_3$. But subsequent researches clearly revealed that beta alumina is non-stoichiometric as prepared and the more appropriate formula should be $(Li/Na_2O)_{1+x} \cdot 11Al_2O_3$ [4-6]. Although it was demonstrated to be non-alumina, the original name of beta alumina is still used generally.

Kummer *et al*. investigated the details of ionic diffusion in beta alumina and discovered the remarkably high conductivity of lithium or sodium ions in 1967 [7, 8]. This discovery directly inspired the concept of high-temperature sodium batteries and during subsequent decades this material has been much studied for applications in energy storage, laser hosts and sensors [4, 9-11].

Beta alumina selectively passes alkali metal ions while blocking other species, including liquid sodium and liquid sulfur. Its conductivity at operating temperatures (250–300 ºC) compares favorably with electrolytes used in conventional battery systems such as sulfuric acid and potassium hydroxide. Ford Motor Company developed the sodium-sulfur battery for a storage device in electric vehicles [12]. As a secondary battery, the Na-S battery can be continuously used, allowing at least 1000 deep charge/discharge cycles. Several commercial installations use this type of battery for load leveling.

With further study on beta alumina, a number of alkali and alkali-earth aluminates are known to belong to beta alumina group, including Li$^+$, K$^+$, Rb$^+$, Cs$^+$, Ca^{2+}, Mg^{2+}, Ba^{2+} and Sr^{2+} beta alumina [13-20]. They were usually prepared from Na-β-alumina by ion exchange method [15] and shared the common features of the crystal structure of original Na-β-alumina. As Li-ion battery is widely used in various fields nowadays, Li-β-alumina draws more attention for its high ionic conductivity at room temperature, especially in the form of film. To make a better study on Li-β-alumina here, it is necessary to fully understand its crystal structure.

Beta alumina group can be subdivided into those members containing a twofold screw axis in unit cell and those containing a threefold screw axis in unit cell. The archetypes of the two subgroups are designated β-alumina (twofold) and β"-alumina (threefold), respectively. The idealized crystal structures of Li-β-alumina and Li-β"-alumina were depicted by using VESTA (Visualization for

Electronic and Structural Analysis) in Figure 1. Both of Li-β-alumina (a) and Li-β"-alumina (b) are characterized by structures composed of alternating slabs of closely-packed oxides (AlO$_4$, AlO$_6$) and loosely-packed layers with a low atom density containing mobile Li ions. Al^{3+} cations occupy both octahedral and tetrahedral interstices in the closely-packed slabs, forming a dense spinel block to prevent Li ions moving along c-axis. The loosely-packed layer supplies enough space for Li ions to move and is therefore named conduction plane. Li-β-alumina contains a mirror plane through the layer of mobile Li ions in the hexagonal unit cell, as shown in Figure 1(a). Li-β"-alumina is stacked according to a threefold screw axis. It contains no mirror plane and has a rhombohedral crystal structure, as shown in Figure 1(b). The unit cell of Li-β"-alumina is 50% larger than that of Li-β-alumina. On the conduction plane of Li-β"-alumina, there is a higher density of Li ions than Li-β-alumina, which can contribute to higher electrical conductivity of Li-β"-alumina. Meanwhile, some Al^{3+} vacancies are caused in Li-β"-alumina due to charge compensation, forming a defective spinel block.

The preparation of beta alumina as polycrystalline ceramics (a tube in battery) has largely dominated the field. However, film electrolyte has attracted considerable attention recently because of its use in advanced thin film Li-ion battery. Reducing the beta alumina thickness to micron range results in a significant drop in area specific resistance. By using film electrolyte, reduction in size/weight of battery is not the only advantage, it also enhances the battery cycle life. To date, most of researches were focused on preparation of beta alumina ceramics in the form of powder or bulk, there being no literatures or reports of Li-β/β"-alumina film. As we know, chemical vapor deposition (CVD) can make uniform film with high purity in the optimal condition. However, Li-β/β"-alumina films have never been obtained by CVD because of high crystallization temperature, high vapor pressure of Li and high reactivity of Li precursor. Thus, decreasing the preparation temperature is probably a necessary step to prepare Li-β/β"-alumina film. We have developed laser-assisted CVD (LCVD) using high-power continuous-wave oscillation laser expanded to wide deposition area with a lens. The laser irradiation field during CVD enables us to fabricate films with highly-textured microstructures at relatively low deposition temperature. We reported the high-speed growth of films in various pseudo binary systems, such as BaO–TiO$_2$ and ZrO$_2$–Al$_2$O$_3$, clarifying those phase formation relationships and microstructures by LCVD. We also reported the preparation of Li-Al-O films, such as LiAl$_5$O$_8$ and Li$_5$AlO$_4$, at low deposition temperature by laser chemical vapor deposition (LCVD). In the present study, we report the process of synthesis of Li-β-alumina film and study its microstructure and electrical property.
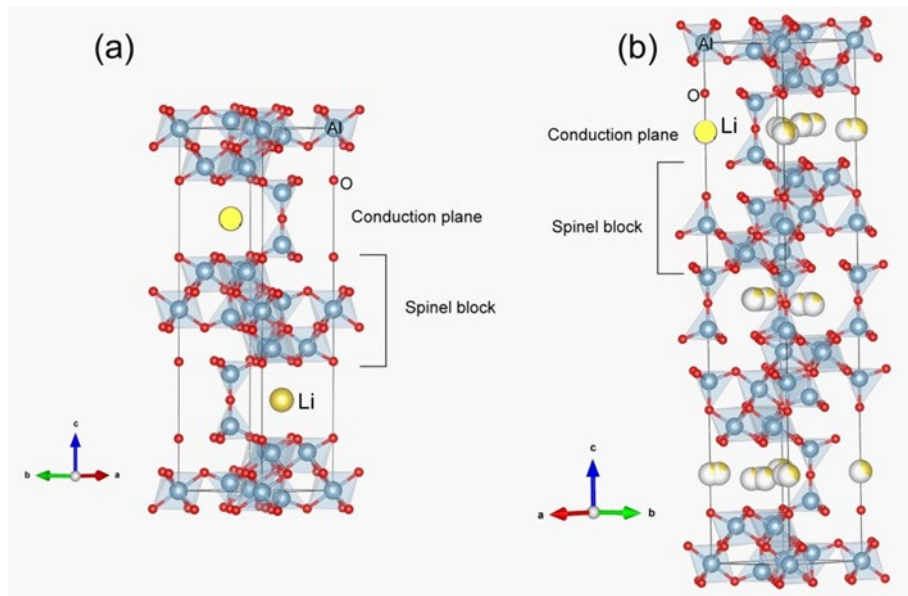
Figure 1: Crystal structures of Li-β-alumina (a) and Li-β"-alumina (b).

2. Experimental details

Laser chemical vapor deposition (laser CVD) is a deposition technique for films of various materials by introducing activated field with laser irradiation for chemical reaction. The schematic of

CVD apparatus with double lasers was shown in Figure 2. A cold-wall chamber was constructed as the main part of laser CVD setup. Diode and YAG lasers with continuous wave were employed. AlN was used as substrate because of high thermal conductivity. Precursors were evaporated in the furnace and their vapors were transported to the reaction region (substrate) by Ar carrier gas. Before deposition, the substrate was preliminarily pre-heated and irradiated by the diode laser through a quartz window at an incident angle of 45°. The chemical reaction on the substrate surface was thus activated greatly, which decreased the preparation temperature and accelerated the deposition of films.
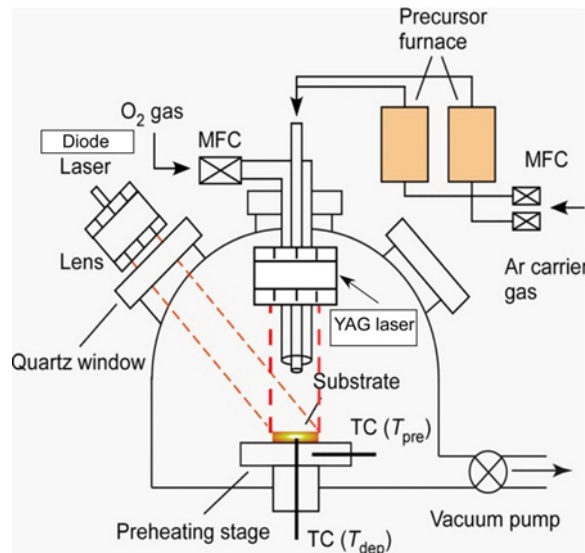
Figure 2: Schematic of laser CVD apparatus.

Deposition temperature was controlled by adjusting laser power output (P_L) from 50 to 200 W and irradiation spot size of laser was 15 mm in a diameter. AlN substrate (10 mm × 10 mm × 1mm) was put on a hot stage pre-heated at 873 K (T_{pre}). The temperature distribution in the substrate was within several K. The deposition temperature (T_{dep}) was measured by a thermocouple beneath the substrate. The vaporization temperature (T_{vap}) of aluminum acetylacetonate (Al(acac)$_3$) precursor was fixed at 443 K, while that of lithium dipivaloymethanate (Li(dpm)) precursor was changed from 573 to 873 K. The molar ratio of evaporated Li to Al precursor ($R_{Li/Al}$) was regulated by changing the T_{vap} of Li(dpm) precursor. The precursor vapors and O$_2$ gas were separately introduced into the reaction chamber through a double-tube nozzle. The flow rates of Ar carrier gas for each precursor and O$_2$ gas were fixed at 8.3×10^{-7} and 1.7×10^{-6} m^3 s^{-1}, respectively. The temperature of all the gas lines was maintained at 663 K to prevent the condensation of precursor vapors during the transportation. The total pressure (P_{tot}) in the reaction chamber was changed from 600 to 1000 Pa. The deposition time was 40—600 s.

The deposition rate (R_{dep}) was calculated from the film thickness per deposition time. The crystalline phase was examined by X-ray diffraction (XRD; Rigaku: RAD-2C). The microstructure was observed by scanning electron microscopy (SEM; Hitachi: S-3100H) and transmission electron microscopy (TEM; JEM-2100HC). Schematic of the crystal structure of Li-β-alumina was drawn by the VESTA program.

The impedance measurements were carried out at 373 to 1173 K in air using a Solartron 1296 frequency analyzer coupled to a 1286 electrochemistry interface over the frequency range 10^{-2} to 10^7 Hz. The bottom electrode of Li-β-alumina films was Pt that deposited on AlN substrate by a D.C. sputter at 1073 K for 900 s with the thickness of 200 nm. After deposition of Li-β-alumina films on the unmasked Pt layer, a gold wire was sticked on the film by the gold paste 0.5 mm in diameter and annealed at 1073 K for 7.2 ks in air as upper electrode. Before each impedance measurement the cell was kept at the testing temperature for at least 30 min to allow thermal equilibration.

3. Results and Discussion

Figure 3 shows XRD patterns of Li-β-alumina films prepared at $T_{dep} = 1100$ K, $P_{tot} = 600$ Pa, $R_{Li/Al} = 20$ (a); $T_{dep} = 1120$ K, $P_{tot} = 600$ Pa, $R_{Li/Al} = 25$ (b); $T_{dep} = 1120$ K, $P_{tot} = 1000$ Pa, $R_{Li/Al} = 25$ (c); $T_{dep} = 1150$ K, $P_{tot} = 600$ Pa, $R_{Li/Al} = 30$ (d); $T_{dep} = 1250$ K, $P_{tot} = 600$ Pa, $R_{Li/Al} = 30$ (e). In Fig.3(a, b, d) Relative intensity of the (001) reflection peak at 7.8° was significantly higher than that of a powder

pattern (JCPDF#72-0587), implying the (001) orientation. The *TC* value of the (001) orientation was 9.2. And the films prepared at high total pressure or high deposition temperature had non-orientation, as shown in Fig.3(c, e). Since the Li (dpm) precursor is reactive in a gas phase and on the CVD chamber wall, the exhausted $R_{Li/Al}$ ratio was significantly higher than the stoichiometric ratio of Li/Al for Li-β-alumina (0.1–0.2). At $R_{Li/Al}$=20—30, Li-β-alumina was formed above 600 Pa. However, no Li-β-alumina phase was formed at $R_{Li/Al}$ lower than 20.
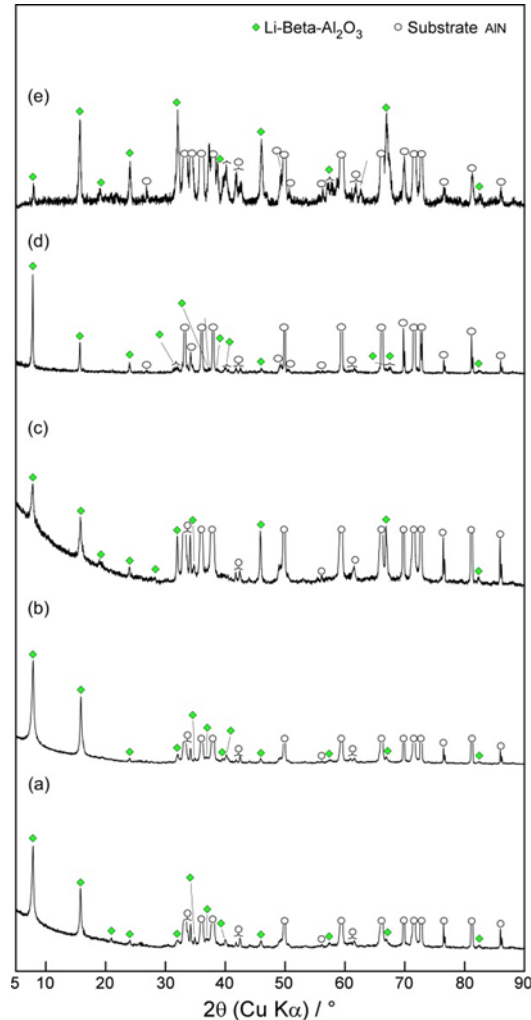
Figure 3: XRD patterns of Li-β-alumina films prepared at various conditions: T_{dep} = 1100 K, P_{tot} = 600 Pa, $R_{Li/Al}$ = 20 (a); T_{dep} = 1120 K, P_{tot} = 600 Pa, $R_{Li/Al}$ = 25 (b); T_{dep} = 1120 K, P_{tot} = 1000 Pa, $R_{Li/Al}$ = 25 (c); T_{dep} = 1150 K, P_{tot} = 600 Pa, $R_{Li/Al}$ = 30 (d); T_{dep} = 1250 K, P_{tot} = 600 Pa, $R_{Li/Al}$ = 30 (e).

Fig. 4 shows the XPS spectrum of the Li-β-alumina film prepared at $R_{Li/Al}$=30. The wide scan spectrum exhibited photoelectron peaks assigned to the constituent elements of Li-β-alumina (i.e. Li 1 s at 55 eV, O 1 s at 530 eV, and Al 2p at 73 eV). Minor peaks arising from the argon embedded upon the sputtering procedure and carbon (below 5 mol%) were also detected. The C peaks originated from the residual carbonates formed upon air exposure to air or from metal organic precursors. The chemical composition estimated by the photoelectron peak area was $Li_{1.0}Al_{5.8}O_{9.2}$. This Li/Al ratio of the film composition (Li/Al = 1/5.8) was considerably lower than $R_{Li/Al}$ (=30), indicating the depletion of the Li vapor source in a gaseous phase.
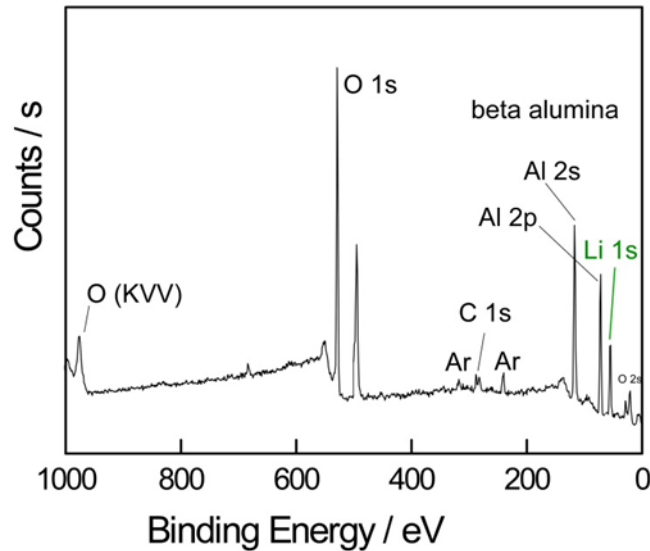
Figure 4: XPS photoelectron spectra of Li-β-alumina film deposited at T_{dep} = 1150 K, P_{tot} = 600 Pa and $R_{Li/Al}$ = 30.

The surface and cross section of Li-β-alumina films prepared at different conditions were depicted in Figure 5. The Li-β-alumina films prepared at P_{tot}= 600 Pa consisted of bulk grains in the grain sizes of about 3–5 μm and the cross section was granular structure, as shown in Fig. 5(a, c). Flake-like Li-β-alumina films were obtained at P_{tot}= 1000 Pa, as shown in Fig. 5(b, d). The deposition rates of Li-β-alumina films were 10–30 μm h^{-1}. Figure 6 shows the bright field TEM image of the Li-β-alumina film grown at $R_{Li/Al}$=30. As is seen, the platelet grains were elongated from the substrate. The selected area electron diffraction (SAED) pattern corresponds to the grain designated in cycle. This indicated that the (0001) planes of the Li-β-alumina grain were inclined from the substrate. The Li-β-alumina film had grains with the conduction planes vertical to the substrate surface, where the Li ions were arrayed in the film thickness direction. In the presence of electric field, the Li ions can two-dimensionally migrate along the conduction planes. Therefore, it is desirable to have the crystal orientations the conduction planes parallel to current flows for use as electrolytes in the batteries.
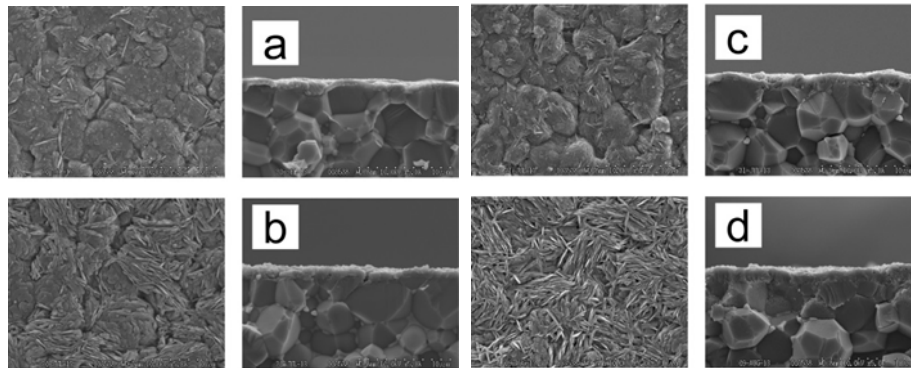
Figure 5: Surface and cross-sectional microstructures of Li-β-alumina films prepared at (a) T_{dep} = 1150 K, $R_{Li/Al}$= 20, P_{tot}= 600 Pa; (b) T_{dep} = 1150 K, $R_{Li/Al}$= 30, P_{tot}= 1000 Pa; (c) T_{dep} = 1120 K, $R_{Li/Al}$= 20, P_{tot}= 600 Pa; (d) T_{dep} = 1120 K, $R_{Li/Al}$= 30, P_{tot}= 1000 Pa.

Figure 7 shows the complex impedance plots of Li-β-alumina film at room temperature (298 K). The scattered points at bottom right corner presents the amplified high-frequency area. The complex impedance of Li-β-alumina film consisted of a semicircle at high frequency ($10^5 – 10^7$ Hz), an arc appearing from $10^2 – 10^5$ Hz and an inclined straight line at low frequency. It could be deduced that the electrical processes arise basically due to the contribution from bulk and electrolyte/electrode interface and additional grain boundary effect for Li-β-alumina polycrystalline film. Calculated from the impedance plot, Li-β-alumina film showed an electrical conductivity of $2×10^{-4}$ S/cm at room temperature, much higher than those of other solid electrolytes such as LISICON ($2×10^{-6}$ S/cm at 323 K) and Li-Zr-Ta-P-O ceramic ($4×10^{-6}$ S/cm at 298 K).
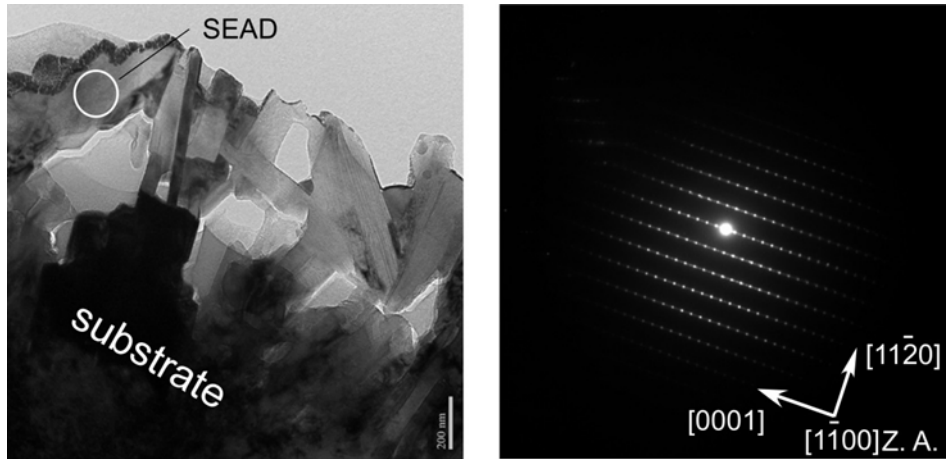
Figure 6: TEM bright field image and electron diffraction pattern of Li-β-alumina film deposited at T_{dep}= 1150 K, $R_{Li/Al}$ = 30 and P_{tot} = 800 Pa.
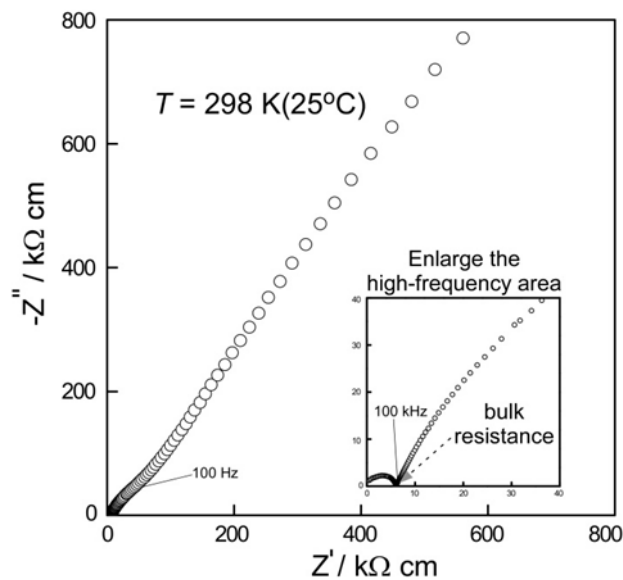
Figure 7: Complex impedance of Li-β-alumina film at 298 K.

4. Conclusions

Li-β-alumina film was first grown onto AlN substrates by laser CVD at T_{dep}=1100K–1300 K, $R_{Li/Al}$=20–50 and P_{tot}=600–1000 Pa. The Li-β-alumina film deposited at P_{tot} = 600 Pa consisted of bulk grains in the grain sizes of about 3–5 μm with granular cross section, while that deposited at P_{tot}=1000 Pa showed a hexagonally faceted platelet morphology (flake-like), containing grains with (0001) planes almost vertical to the substrate surface. The R_{dep} of the Li-β-alumina films reached 30 μm h^{-1} at T_{dep}=1225 K, $R_{Li/Al}$=30 and P_{tot}=600 Pa. The as-prepared Li-β-alumina film showed an electrical conductivity of 2×10^{-4} S/cm at room temperature, significantly higher than those of other solid electrolytes.

Acknowledgements

References

[1] R.R. Ridgway, A.A. Klein, W.J. O'Leary. The Preparation and Properties of So-Called "Beta Alumina". Transactions of the Electrochemical Society, 1936, 70: 71-88.

[2] R.M. Dell, P.T. Moseley. Beta-alumina electrolyte for use in sodium/sulphur batteries Part 2: Manufacture and use. Journal of Power Sources, 1981, 7: 45-63.

[3] R.M. Dell, P.T. Moseley. Beta-alumina electrolyte for use in sodium/sulphur batteries: Part I: Fundamental properties. Journal of Power Sources, 1981, 6:143-160.

[4] X. Lu, G. Xia, J.P. Lemmon, Z. Yang. Advanced materials for sodium-beta alumina batteries: Status, challenges and perspectives. Journal of Power Sources, 2010, 195: 2431-2442.

[5] Sung-Tae Lee, Ki-Moon Lee, Dae-Han Lee, Jung-Rim Haw, S.-K. Lim. Analysis of the phase formation of Na-β/β''-aluminas using MgO and Li$_2$O as phase stabilizers. Journal of Ceramic Processing Research, 2011, 12: 38-45.

[6] H. Mituo. Lattice constants of non-stoichiometric beta-alumina. Materials Research Bulletin, 1971, 6: 461-464.

[7] Yungfang Yu Yao, J.T. Kummer. Topotactical reactions with ferrimagnetic oxides having hexagonal crystal structures. J. Inorg. Nucl. Chem., 1967, 29: 2453-2475.

[8] J.T. Kummer. β-Alumina electrolytes. Progress in Solid State Chemistry, 1972, 7: 141-175.

[9] K. Tanaka. Concept design of solar thermal receiver using alkali metal thermal to electric converter (AMTEC). Current Applied Physics, 2010, 10: 254-256.

[10] J.A. Jeevarajan. Battery Safety. Safety Design for Space Systems, 2009, 11: 507-548.

[11] G. He, T. Goto, T. Narushima, Y. Iguchi. Electrical conductivity of alkaline-earth metal β-aluminas and their application to a CO$_2$ gas sensor. Solid State Ionics, 1999, 121: 313-319.

[12] R. Holze. Secondary Batteries–High Temperature Systems | Sodium–Sulfur. Encyclopedia of Electrochemical Power Sources, 2009, 1: 302-311.

[13] M.M. Bućko, M. Cichocińska. Preparation of Ca-β''-Al$_2$O$_3$ from alumina gel. Journal of the European Ceramic Society, 1996, 16: 79-84.

[14] J.-H. Koh, N. Weber, A.V. Virkar. Synthesis of lithium-beta-alumina by various ion-exchange and conversion processes. Solid State Ionics, 2012, 220: 32-38.

[15] V. Jayaraman, G. Periaswami, T.R.N. Kutty. Preparation of lithium β-alumina by the ionexchange reaction. Mater. Res. Bull., 1998, 33: 1811-1820.

[16] A.Y. Zhang, T. Akashi, B.P. Zhang, T. Goto, T. Zhang. Electrical conductivity and ionic transport number of Sr β-alumina single crystals prepared by a floating zone method. Solid State Ionics, 2005, 176: 2319-2323.

[17] A.Y. Zhang, T. Akashi, T. Goto. Electrical conductivity of non-stoichiometric Sr β-alumina single crystals prepared by a floating zone method. Solid State Ionics, 2003, 156: 425-431.

[18] C. Kun Kuo, P.S. Nicholson. The growth of K-β-Al$_2$O$_3$ single-crystal films on single-crystal α-Al$_2$O$_3$ substrates. Solid State Ionics, 1994, 73: 297-301.

[19] S. Yamaguchi, K. Kimura, M. Tange, Y. Iguchi, A. Imai. Ionic conduction in Sr hexa-aluminate with β-alumina structure. Solid State Ionics, 1988, 26: 183-188.

[20] I. Atsuo, H. Mituo. Ionic Conduction of Impurity-Doped β-Alumina Ceramics. Japanese Journal of Applied Physics, 1972, 11: 180.